

# Integrating a Silicon Solar Cell with a Triboelectric Nanogenerator *via* a Mutual Electrode for Harvesting Energy from Sunlight and Raindrops

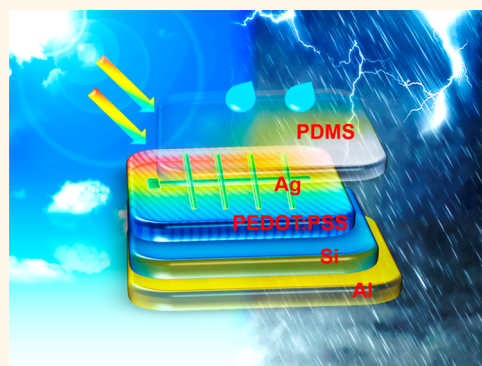
Yuqiang Liu,<sup>†</sup> Na Sun,<sup>†</sup> Jiawei Liu, Zhen Wen,<sup>\*</sup> Xuhui Sun,<sup>\*</sup> Shuit-Tong Lee,<sup>‡</sup> and Baoquan Sun<sup>\*</sup>

Jiangsu Key Laboratory for Carbon-Based Functional Materials and Devices, Institute of Functional Nano & Soft Materials (FUNSOM), Joint International Research Laboratory of Carbon-Based Functional Materials and Devices, Soochow University, Suzhou 215123, China

## Supporting Information

**ABSTRACT:** Solar cells, as promising devices for converting light into electricity, have a dramatically reduced performance on rainy days. Here, an energy harvesting structure that integrates a solar cell and a triboelectric nanogenerator (TENG) device is built to realize power generation from both sunlight and raindrops. A heterojunction silicon (Si) solar cell is integrated with a TENG by a mutual electrode of a poly(3,4-ethylenedioxythiophene):poly(styrenesulfonate) (PEDOT:PSS) film. Regarding the solar cell, imprinted PEDOT:PSS is used to reduce light reflection, which leads to an enhanced short-circuit current density. A single-electrode-mode water-drop TENG on the solar cell is built by combining imprinted polydimethylsiloxane (PDMS) as a triboelectric material combined with a PEDOT:PSS layer as an electrode. The increasing contact area between the imprinted PDMS and water drops greatly improves the output of the TENG with a peak short-circuit current of ~33.0 nA and a peak open-circuit voltage of ~2.14 V, respectively. The hybrid energy harvesting system integrated electrode configuration can combine the advantages of high current level of a solar cell and high voltage of a TENG device, promising an efficient approach to collect energy from the environment in different weather conditions.

**KEYWORDS:** *integrated device, silicon solar cell, triboelectric nanogenerator, energy harvesting, shared electrode configuration*



Solar cells have become one of the most widespread solutions in the crisis issues of the environment and energy.<sup>1</sup> However, the power generation from a solar cell is affected by various weather conditions; for example, rainy weather deteriorates its performance. The intermittent and unpredictable nature of solar energy is an inevitable challenge for its expansion as a reliable power supply system. Scavenging alternative energy from the environment with different types of energy harvesters, to compensate for the insufficient part, is urgent.<sup>2–4</sup>

Recently, triboelectric nanogenerators (TENGs) have been widely demonstrated as energy collecting systems to harvest mechanical energy into electricity power.<sup>5–8</sup> It is possible to integrate solar cells with TENGs to realize solar energy harvesting during sunny days and raindrop energy in rainy conditions. For example, a charge-enriched reduced graphene oxide film<sup>9</sup> or a transparent poly(dimethylsiloxane) (PDMS) layer<sup>10–12</sup> is used to cover the surface of a solar cell to fabricate a water-drop power system in order to generate electricity from

both solar and raindrop energy. These devices achieve a promising energy collection in rainy conditions. However, these works merely put a pseudocapacitor or nanogenerator on a solar cell, which is not a compact device. Two independent energy harvesting units are separated by an insulating layer (polyethylene terephthalate, glass, etc.), which requires an extra conducting wire to connect the two devices for realizing electricity output simultaneously. Although the hybrid energy harvesting system is expected to combine the advantages of high current level of a solar cell and high voltage of a TENG device, unfortunately, the thick and complex layered TENG with a large electric resistance as well as poor transparency would dramatically deteriorate the output current level of a solar cell. Therefore, it is indispensable to optimize the integrated device structure to reduce the output loss of the

Received: January 16, 2018

Accepted: February 14, 2018

Published: February 14, 2018

solar cell without sacrificing the TENG device performance. At present, it is challenging to integrate a solar cell with a TENG device due to the lack of an appropriate mutual joint component.

In various solar cells, a silicon (Si)/organic hybrid solar cell fabricated by the conductive polymer poly(3,4-ethylenedioxythiophene):poly(styrenesulfonate) (PEDOT:PSS) deposited on a Si wafer has attracted wide interest because of its potential high efficiency.<sup>13–18</sup> So far, strategies of an electron (hole) blocking layer,<sup>19</sup> surface passivation,<sup>20</sup> an antireflection layer,<sup>21</sup> modification of PEDOT:PSS,<sup>22</sup> and texturing the Si nanostructure<sup>23</sup> have been proposed to increase the performance of Si/PEDOT:PSS solar cells, and a power conversion efficiency (PCE) of more than 17% has been achieved.<sup>24</sup> Among these methods, textured Si, which mainly includes nanocones,<sup>25</sup> nanowires,<sup>26</sup> nanopillars,<sup>27</sup> nanotubes,<sup>28</sup> nanoholes,<sup>29</sup> pyramids,<sup>30</sup> and composite nanostructures,<sup>31</sup> is crucial to enhance sunlight harvesting and then boost the short-circuit current density ( $J_{sc}$ ). However, textured Si displays a large surface/volume ratio, which results in serious charge recombination.<sup>32,33</sup> Being similar to textured Si, the surface structure of PDMS could further improve the output performance of a TENG owing to the much larger contact area between water and the triboelectric layer. However, PDMS layer texturing could also encounter complicated fabrication processes. How to specially design and process the textured structure to achieve the high-efficiency dual function of being a protection layer and a water-drop TENG still remains a challenge.

In this work, we propose an energy harvesting system with a digital video disk (DVD) pattern by integrating a heterojunction Si solar cell and a single-electrode-mode TENG, where the PEDOT:PSS layer acts as a mutual component for both devices. The Si/PEDOT:PSS heterojunction allows generating power from solar energy; PEDOT:PSS/PDMS is conducted the raindrop-driven TENG operating from water drops. Solar cells with imprinted PEDOT:PSS achieve a PCE of 13.6%. When an imprinted-PDMS template contacts the PEDOT:PSS layer, an integrated TENG is constructed with a short-circuit current ( $I_{sc}$ ) of  $\sim 33.0$  nA and an open-circuit voltage ( $V_{oc}^{TENG}$ ) of  $\sim 2.14$  V under the simulated raindrop condition. Finally, the Si solar cell–TENG integrated systems achieve a synthetic power output, which demonstrates a promising method for enhancing energy harvesting in different weather conditions.

## RESULTS AND DISCUSSION

Excellent operability and flexibility of PDMS and PEDOT:PSS films allow them to be convenient for imprinting through template methods,<sup>34</sup> as shown in Figure S1. A commercial DVD is employed as the initial substrate (Figure S1a), and a PDMS solution is coated onto the surface of the disk followed by heating solidification. Subsequently, the solidified PDMS film is peeled off to get the imprinted-PDMS template with inverse disk structure (Figure S1b and c). To fabricate an imprinted-PEDOT:PSS film, the PDMS module is placed onto the surface of the PEDOT:PSS layer with a mild short annealing process (Figure S1d); then PDMS is lifted off and an imprinted-PEDOT:PSS layer is acquired (Figure S1e). The detailed process is demonstrated in the Experimental Methods section.

A photograph of an imprinted-PDMS slice in Figure 1a clearly shows a uniform film quality. It is easy to transfer this structure to another soft matrix. As shown in Figure 1b, the

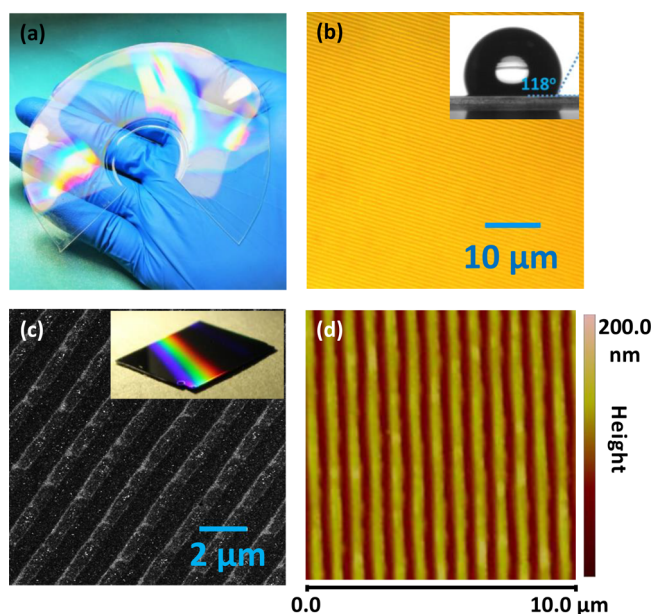


**Figure 1.** Typical characterizations of an imprinted film. (a) Photograph of an imprinted-PDMS film; (b) optical microscope photograph of imprinted-PDMS film; inset photograph is the contact angle of water on an imprinted-PDMS film; (c) SEM image of imprinted-PEDOT:PSS on a Si substrate; inset is a photograph of an imprinted-PEDOT:PSS layer on a Si substrate; (d) AFM height image of an imprinted-PEDOT:PSS film on a Si substrate.

pattern of the DVD has been successfully transferred onto the PDMS film, which generates the order of colors in a rainbow due to the light interference in the patterned film. The inset image in Figure 1b shows the contact angle ( $\sim 118^\circ$ ) of water on an imprinted-PDMS film, indicating the hydrophobic property of the film. This is favorable for the water-drop TENG device because the raindrop water would not stick to the substrate. In addition, the stability of solar cells would benefit from the hydrophobic surface, since it could prevent water from penetrating the Si. Figure S2 and Figure 1c are optical microscope and scanning electron microscope (SEM) images of the imprinted-PEDOT:PSS film on a Si substrate, respectively. Both images show that the surface of the PEDOT:PSS layer changes into grating structures with a period of width of  $\sim 400$  nm after the imprinting process. The depth profile of the structure is further investigated by atomic force microscopy (AFM). As exhibited in Figure 1d of the AFM height image and Figure S3 of the cross-sectional line profile of the AFM topography image, the PEDOT:PSS layer clearly displays a well-organized pattern with a depth of  $\sim 75$  nm. The ordered nanostructure for the imprinted-PEDOT:PSS layer on Si results in the order of colors in a rainbow (inset in Figure 1c). In fact, imprinted PDMS and PEDOT:PSS not only present a colorful visual effect but also enhance the hybrid device's performance, which will be demonstrated in the following discussion.

The structure of a Si/organic heterojunction solar cell based on Ag grids/PEDOT:PSS/Si/Al is shown in Figure 2a. PEDOT:PSS, with a high work function, is contacted with an n-type Si wafer to form a heterojunction, where a strong inversion layer is generated,<sup>16,35</sup> as illustrated in the band energy scheme of Figure 2b. As a result, a larger built-in potential ( $V_{bi}$ ) is generated. When the incident photons transmitted by the PEDOT:PSS layer are absorbed by Si, the

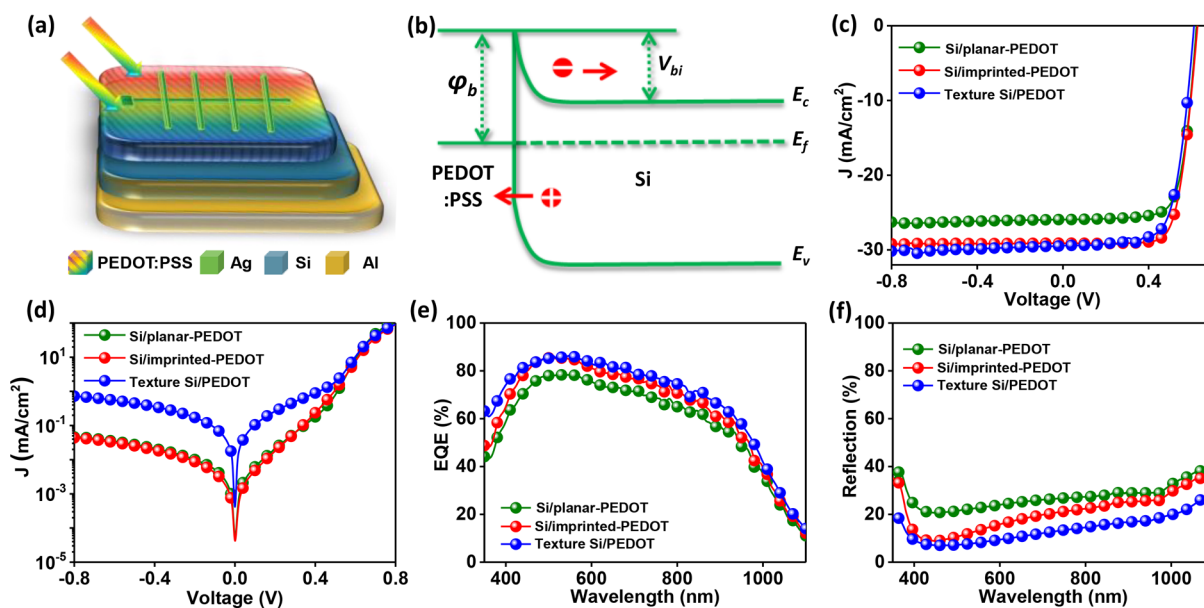


**Figure 2.** Solar cell structure and general performance of Si/PEDOT:PSS hybrid solar cells for harvesting solar energy. (a) Cartoon image of a device structure of the solar cell. (b) Band energy diagram of the solar cells.  $\Phi_b$ : Shockley barrier,  $V_{bi}$ : built-in potential,  $E_c$ : conductive band,  $E_f$ : Fermi level,  $E_v$ : valence band. (c)  $J$ - $V$  curves of the solar cells under illumination of simulated AM 1.5G ( $100 \text{ mW/cm}^2$ ) solar spectra. (d)  $J$ - $V$  curves of the solar cells in the dark. (e) EQE curves of the solar cells. (f) Reflectance spectra of textured-Si/PEDOT:PSS, Si/planar-PEDOT:PSS, and Si/imprinted-PEDOT:PSS.

photogenerated holes and electrons are swept toward the respective electrodes driven by the  $V_{bi}$ . Furthermore, the higher energy barrier ( $\Phi_b$ ) accompanied by the  $V_{bi}$  becomes an obstacle to impede the reverse carrier flow and then reduces the possibility of carrier recombination. When the anode (Ag grids) and cathode (Al) are connected with a load, the device would be under operation conditions; that is, solar power is converted into electric energy.

The current density–voltage ( $J$ - $V$ ) curves of solar cells under illumination from a simulated solar spectrum are shown in Figure 2c, and the detailed electrical output characteristics are summarized in Table 1. A device based on a flat

**Table 1. Electrical Output Characteristics of Different Solar Cells**

device structure	$V_{oc}^{PV}$ (V)	$J_{sc}$ ( $\text{mA/cm}^2$ )	$J_{sc}^*$ ( $\text{mA/cm}^2$ ) <sup>a</sup>	FF	PCE (%)
Si/planar-PEDOT:PSS	0.625	25.8	26.7	0.746	12.0
textured-Si/PEDOT:PSS	0.612	29.4	30.2	0.702	12.6
Si/imprinted-PEDOT:PSS	0.628	29.1	28.9	0.745	13.6

<sup>a</sup> $J_{sc}^*$ : short-circuit current density calculated by integrating EQE curves with a standard AM 1.5G solar spectrum.

PEDOT:PSS layer on planar Si (Si/planar PEDOT:PSS) exhibits an open-circuit voltage ( $V_{oc}^{PV}$ ) of 0.625 V, a  $J_{sc}$  of  $25.8 \text{ mA/cm}^2$ , a fill factor (FF) of 0.746, and a PCE of 12.0%. A device based on imprinted PEDOT:PSS on planar Si (Si/imprint PEDOT:PSS) achieves a  $V_{oc}^{PV}$  of 0.628, a  $J_{sc}$  of  $29.1 \text{ mA/cm}^2$ , an FF of 0.745, and a PCE of 13.6%. To further identify the feasibility of an imprinted-PEDOT:PSS layer, a solar cell of a flat PEDOT:PSS layer combined with textured Si (Figure S4) is also fabricated (textured-Si/PEDOT:PSS), which exhibits a  $V_{oc}^{PV}$  of 0.612 V, a  $J_{sc}$  of  $29.4 \text{ mA/cm}^2$ , an FF of 0.702, and a

PCE of 12.6%. The  $J_{sc}$  of the Si/imprinted-PEDOT:PSS device is improved more than 12% compared to that of a device without a textured structure, which is verified by the external quantum efficiency (EQE) in Figure 2e. The improvement of  $J_{sc}$  is mainly ascribed to the grating structures on the PEDOT:PSS layer, which dramatically suppress the reflection ratio. As demonstrated by the reflection spectra in Figure 2f, the Si/imprinted-PEDOT:PSS sample displays a broad antireflection range, which is superimposed with its EQE spectrum. Therefore, the Si/organic solar cell with an imprinted-PEDOT:PSS layer could increase the light harvesting ratio and subsequently enhance the  $J_{sc}$  level. Meanwhile, textured-Si/PEDOT:PSS also exhibits a higher  $J_{sc}$  of  $29.4 \text{ mA/cm}^2$ , since textured Si could achieve better light trapping as well. However, the solar cells based on the textured Si show a lower  $V_{oc}^{PV}$ , which is ascribed to increased surface charge recombination at the Si surface due to an enlarged surface/volume ratio.

There is no obvious difference in the  $V_{oc}^{PV}$  between Si/planar-PEDOT:PSS and Si/imprinted-PEDOT:PSS devices, while both of them are higher than that of the textured-Si/PEDOT:PSS one (0.612 V). According to Figure 2d of  $J$ - $V$  curves in the dark, the devices based on a planar Si substrate with or without an imprinted structure yield a parallel reverse saturation current density ( $J_0$ ) level, which reveals their similar  $V_{oc}^{PV}$ , since  $V_{oc}^{PV}$  is correlated with  $J_0$  according to the following equation:<sup>36</sup>

$$V_{oc}^{PV} = \frac{KT}{q} \ln \left( \frac{J_{sc}}{J_0} + 1 \right)$$

where  $K$  is the Boltzmann constant,  $T$  is temperature, and  $q$  is electron charge. However, the device on the textured Si exhibits an inferior diode property that is ascribed to increased carrier recombination due to the large Si surface/volume ratio.<sup>32</sup> Hence, the textured-Si/PEDOT:PSS yields a lower  $V_{oc}^{PV}$ . In addition, because the carrier recombination could reduce the  $J_{sc}$

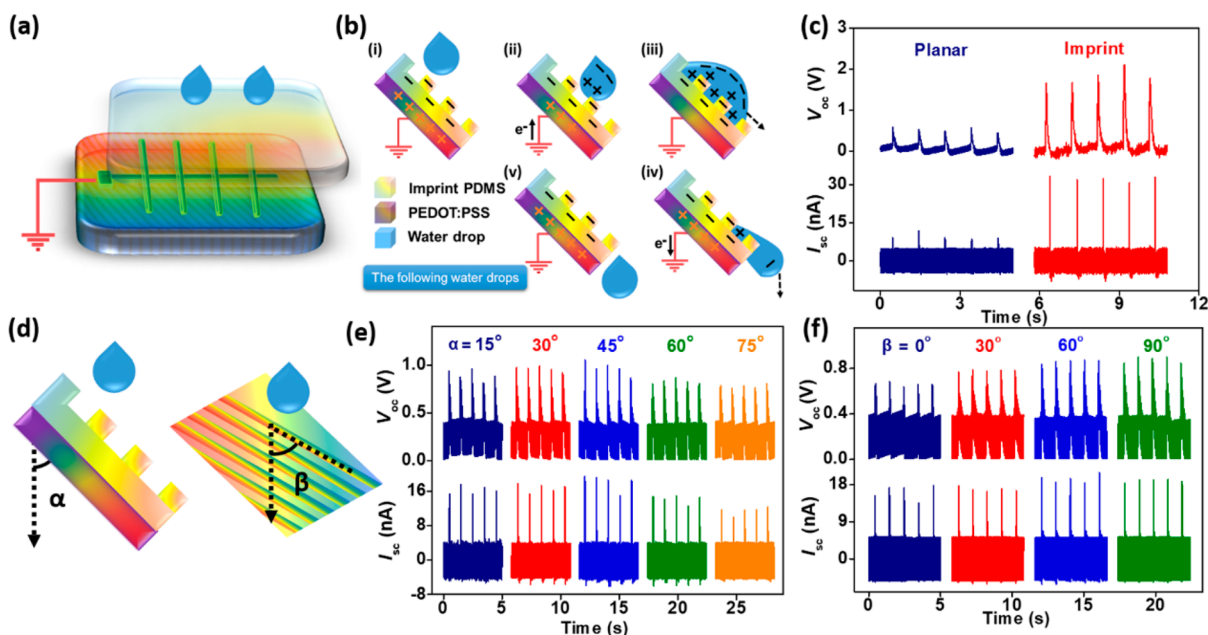


**Figure 3.** TENG device structure and general performance of the TENG for harvesting mechanical energy from water drops. (a) Schematic illustration of a typical TENG structure. (b) Working mechanism of TENG. (c)  $V_{oc}^{TENG}$  and  $I_{sc}$  outputs of a TENG with or without surface imprint. (d) Schematic illustration of angle  $\alpha$  between the water dripping direction and the device and the angle  $\beta$  between the water dripping direction and the imprinted structure. (e)  $V_{oc}^{TENG}$  and  $I_{sc}$  outputs of a TENG under different  $\alpha$ . (f)  $V_{oc}^{TENG}$  and  $I_{sc}$  outputs of a TENG under different  $\beta$ .

the device based on the textured Si with a lower reflection ratio does not promise a higher  $J_{sc}$  compared with the device based on Si/imprinted-PEDOT:PSS. Effective minority carrier lifetime ( $\tau_{eff}$ ) mapping measurements for different Si substrates are conducted to evaluate the surface recombination velocity, as shown in Figure S5. The  $\tau_{eff}$  of textured Si, textured-Si/PEDOT:PSS, planar Si, planar-Si/PEDOT:PSS, and planar-Si/imprinted-PEDOT:PSS are 10, 24, 37, 62, and 60  $\mu$ s, respectively. The textured-Si sample displays the lowest  $\tau_{eff}$  of  $\sim 10$   $\mu$ s because of its large surface/volume ratio. When PEDOT:PSS is deposited on a textured-Si surface, the  $\tau_{eff}$  could be improved to  $\sim 24$   $\mu$ s, which is ascribed to a surface passivation effect from the PEDOT:PSS layer.<sup>15,33</sup> However, both samples based on textured Si (without or with PEDOT:PSS) display shorter  $\tau_{eff}$  than the planar-Si sample. Moreover, planar-Si/PEDOT:PSS with or without imprinting displays similar  $\tau_{eff}$ , in other words, the imprinted-PEDOT:PSS does not introduce any trap sites on the Si surface. The higher  $\tau_{eff}$  is favorable for higher  $V_{oc}^{PV}$  and  $J_{sc}$ . Consequently, the imprinted-PEDOT:PSS layer as an antireflection layer (instead of textured Si) not only enhances light harvesting, which increases the  $J_{sc}$ , but also does not result in any undesirable surface recombination velocity, thus reducing  $V_{oc}^{PV}$ .

To collect the raindrop energy on a rainy day, a TENG is integrated on a heterojunction Si solar cell. A schematic illustration of a raindrop-driven TENG is shown in Figure 3a, which is constructed by an imprinted PDMS as a triboelectric layer and a PEDOT:PSS layer as an electrode. Figure 3b and Figure S6 show the generation process of triboelectric charges based on a single-electrode mode when the TENG harvests the mechanical energy from raindrops that are simulated by water drops.<sup>37–39</sup> When the first water drop contacts the surface of imprinted PDMS (Figure S6, i), the PDMS would be negatively charged due to the triboelectric effect (Figure S6, ii). Meanwhile, the water drop would be positively charged to

maintain electrical neutrality until the charge is saturated in the contact area (Figure S6, iii). As the water drop leaves, the electrons would be transferred from PEDOT:PSS to the ground due to the negative electric potential difference between PEDOT:PSS and the ground (Figure S6, iv) until reaching equilibrium (Figure S6, v). In the following generation process, when subsequent water contacts PDMS, the counterion of the water drop would be attracted by the negative charges on PDMS, which can remain on the surface for a long time (Figure 3b, ii). Meanwhile, the electrons would flow from the ground to PEDOT:PSS due to the positive electric potential difference. Furthermore, the electric double layer would form during the contact and wetting process (Figure 3b, iii).<sup>40</sup> When the water drop leaves the surface of PDMS, the negative electric potential would drive electrons flowing from PEDOT:PSS to the ground, and a new equilibrium would be achieved (Figure 3b, v). With the continuous water drops contacting with the surface of PDMS, a continuous and periodic power output of TENG could be obtained. Both electrical output characteristics from the TENG of PDMS films with or without imprinting are measured. As Figure 3c shows, the  $V_{oc}^{TENG}$  output of the TENG with imprinted PDMS (2.14 V) is about 4 times higher than that of the TENG with planar-PDMS (0.53 V). The short-circuit current ( $I_{sc}$ ) output of the water-drop TENG with imprinted PDMS (33.0 nA) is about 3 times higher than that of the planar PDMS based one (9.5 nA). Hence, the TENG with imprinted PDMS displays superior electric output over the TENG with planar PDMS, which is due to a larger surface area enhancing the output performance.

In order to evaluate the reliability of the raindrops TENG, it is worth investigating the effects of the angle ( $\alpha$ ) between the water dripping direction and the device surface and the angle ( $\beta$ ) between the water dripping direction and the imprinted structure (Figure 3d). Figure 3e shows the measured  $I_{sc}$  and the  $V_{oc}^{TENG}$  of the TENG at different angles  $\alpha$  ranging from 15° to

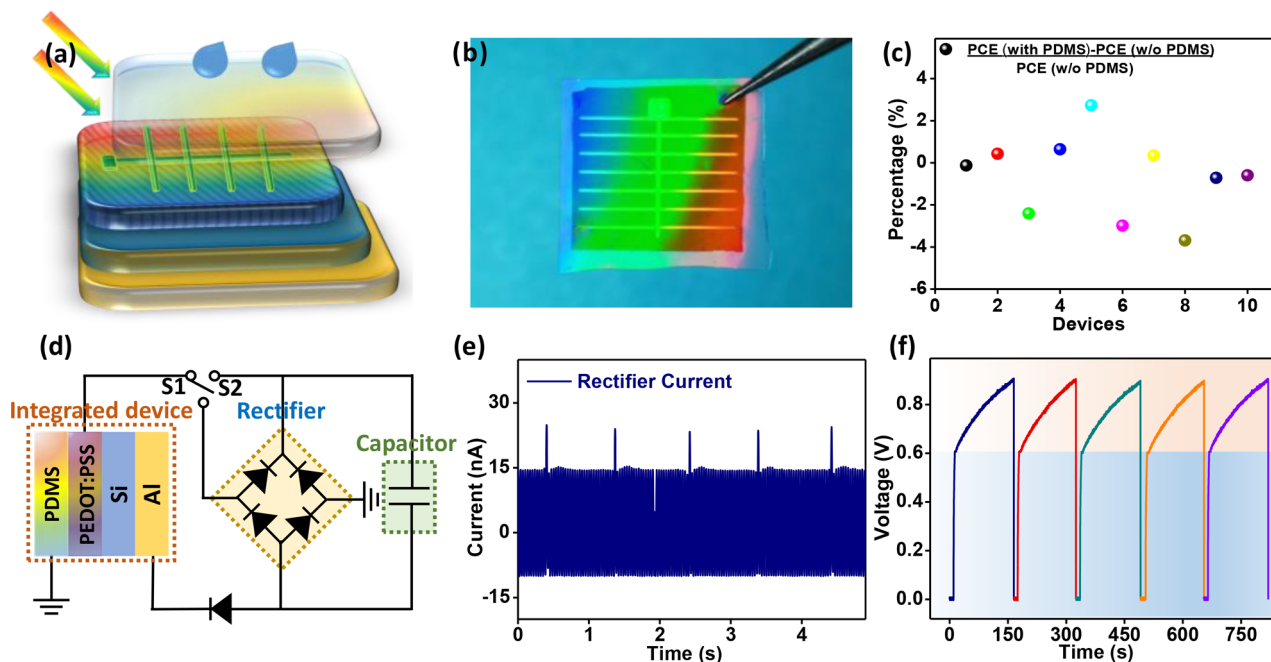


**Figure 4.** Demonstration of the integrated hybrid power system as an energy harvester. (a) Schematic illustration of an integrated device. (b) Photograph of an as-fabricated integrated power system including a TENG and Si solar cell. (c) Variation of the PCE of the solar cells after integrating with a TENG compared with the original one. (d) Circuit diagram of the integrated device. (e) Rectified current output of the TENG. (f)  $V$ - $t$  curves of a capacitor charged by a power system.

$75^\circ$ . There is a slight rise in  $I_{sc}$  and  $V_{oc}^{TENG}$  from about 16.0 nA and 0.90 V at  $15^\circ$  to about 19.7 nA and 0.96 V at  $45^\circ$ , respectively. This is ascribed to the enlarged effective contact surface between water drops and the surface of the TENG with the increase of angle  $\alpha$ . The  $I_{sc}$  and the  $V_{oc}^{TENG}$  of TENG decline substantially when the angle  $\alpha$  reaches  $75^\circ$ , bottoming out at about 11.0 nA and 0.75 V, respectively, because part of the water cannot flow away immediately and stays on the surface, which screens the electrostatic induction effect. The average power was also investigated, as shown in Figure S7, which indicates the same trend of increasing first and then decreasing with the increase of the water dropping angle ( $\alpha$ ). When the angle  $\beta$  is set from  $0^\circ$  to  $90^\circ$  (Figure 3f), the  $I_{sc}$  and the  $V_{oc}^{TENG}$  of the TENG increase slowly from 16.2 nA and 0.64 V to 19.5 nA and 0.88 V, respectively, since the TENG could work well under various angles  $\beta$ , and the larger contact area with the increased angle  $\beta$  leads to an improved output performance. Thus, the imprinted-PDMS TENG has good performance and utility for harvesting the mechanical energy of raindrops.

The aforementioned experiments prove the success of an integrated system of Si/PEDOT:PSS/PDMS. In order to harvest complementary energy from sunlight and raindrops, a hybrid power system is designed, as shown in Figure 4a and b with its schematic structure and its photograph, respectively. When the PDMS film adheres to a solar cell, the change values of PCE of the solar cell are shown in Figure 4c. The result, among 10 device samples, shows that the differences for PCE with and without PDMS are in the range of  $\sim\pm 3\%$ . Therefore, the solar cells still could improve their performance upon integrating with TENG. The reason is mainly owing to the outstanding transmittance of  $\sim 95\%$  (Figure S8) of PDMS films.

The equivalent circuit of the integrated device is illustrated in Figure 4d. The generated current of the TENG is transferred from alternating current (ac) to direct current (dc) by a bridge rectifier for charging one commercial capacitor, and the current

output of the TENG after rectification is  $\sim 24.2$  nA (Figure 4e). The current of the TENG is prevented from going through the solar cell by using a diode. When only the S2 is switched on, as shown in the blue-shaded area of Figure 4f, the voltage of the capacitor could be increased sharply from 0 to 0.6 V in 4 s charged by one solar cell, which is enlarged in Figure S9. However, the voltage of the capacitor would remain at 0.6 V, and the low output limits its reliability and practicability. Therefore, the TENG with a high voltage output could compensate the limitation of the solar cell. When only the S1 is switched on, in the orange-shaded area of Figure 4f, the voltage of the capacitor is near-linearly increased from 0.6 V to 0.9 V while it is charged continuously for about 165 s. Before each charging process, both ends of capacitor are connected to restore the initial state. After five recycling charging processes, the integrating system displays good stability and repeatability. Considering the real applications, the power generation in many raindrops has also been demonstrated, as displayed in Figure S10. The water dropping rate was set at  $13 \text{ mL s}^{-1}$ , and the distance between the TENG and the water shower was set as 40 cm. The  $V_{oc}$ , the  $I_{sc}$ , and the  $Q_{tr}$  of the water-drop TENG reach  $\sim 3.27$  V,  $\sim 0.49 \mu\text{A}$ , and  $\sim 1.05$  nC in the simulated rainy weather, respectively. The maximum average power density can be calculated as  $1.74 \text{ mW/m}^2$ . Thus, the integrated solar cell and TENG system can harvest both solar and raindrop energy.

## CONCLUSION

In conclusion, we have demonstrated an integration device of a solar cell and a TENG through sharing a mutual function electrode of the PEDOT:PSS layer to overcome the output loss of the solar cell, where a simple and key design with an imprinting method is used to improve the output efficiency. Imprinted-PEDOT:PSS deposited on Si exhibits a low

reflection ratio that enhances light harvesting without sacrificing  $V_{oc}^{PV}$  which achieves a higher PCE of 13.6% compared with the textured-Si structure. An imprinted-PDMS film was simply fabricated on PEDOT:PSS to form a TENG that collects raindrops' power with higher outputs of  $\sim 33.0$  nA ( $I_{sc}$ ) and  $\sim 2.14$  V ( $V_{oc}^{TENG}$ ). Finally, an integrated system successfully converts both solar and water-drop energy into electrical power complementarily, which combines the advantage of high current output level of the solar cell and the high voltage output level of the TENG. Our studies demonstrate a new concept in utilization of energy during various weather conditions.

## EXPERIMENTAL METHODS

**PDMS Template Fabrication.** PDMS (Dow Corning, Sylgard 184) was prepared by mixing the two materials with a ratio of 10:1 (w/w) and then casted onto the surface of a DVD followed by heating at 60 °C for 3 h to solidify it. Afterward, the PDMS film was lifted off carefully to get the imprinted-PDMS template with DVD structure.

**Textured-Si Substrate Fabrication.** A cleaned, polished n-type Si wafer (300  $\mu$ m, 0.05–0.1  $\Omega$ /sq) was immersed into aqueous etching solution (hydrofluoric acid (HF) of 4.8 M and silver nitride of 0.02 M) for 5 min. Then, the etched Si sample was cleaned by deionized water followed by dipping into a nitric acid solution and HF solution in sequence. Finally, the Si substrate was immersed into a tetramethylammonium hydroxide (Sigma-Aldrich) aqueous solution (1% w/w) and further cleaned by deionized water.

**Solar Cell and TENG Fabrication.** A PEDOT:PSS (PH 1000, Clevious) solution was mixed with dimethyl sulfoxide (DMSO, Sigma-Aldrich) and Triton (Sigma-Aldrich) of 5 and 1 wt %, respectively. For PEDOT:PSS with imprinted solar cells, the PEDOT:PSS solution was spin-coated onto a planar Si surface at 3000 rpm for 15–20 s; then the textured PDMS was placed onto the surface of the PEDOT:PSS layer followed by annealing at 125 °C for 1 min with a humidity lower than 30%. Finally, PDMS was peeled off and the PEDOT:PSS layer was annealed at 125 °C for 20 min. For PEDOT:PSS without imprinting, the PEDOT:PSS solution was spin-coated on a planar (or textured) Si substrate at 3000 rpm for 1 min and annealed at 125 °C for 20 min. Then a 200-nm-thick Al layer (Ag grids) was thermally evaporated as a cathode (anode) for the solar cells. For the solar cell/TENG hybrid device fabrication, the imprinted-PDMS film with a planar side was placed onto the imprinted-PEDOT:PSS/Si solar cells. Finally, the whole device was heated at 60 °C for 5 min. All the experiments of the TENG test were conducted under the same dripping height of 5 cm, each water drop having a volume of 20  $\mu$ L and dripping frequency of 1 Hz.

**Characterization.** The morphology, transmittance, and hydrophobic properties of imprinted-PDMS were characterized by a fluorescence optical microscope (Leica DM4000M), a UV–vis spectrophotometer (PerkinElmer Lambda750), and a contact angle measurement facility (DataPhysics OCA), respectively. The structure and morphology of the imprinted-PEDOT:PSS layer were investigated by an AFM (Veeco Multimode V) and an SEM (Zeiss Spira55). The textured-Si surface was measured by an SEM (Zeiss Spira55). The minority carrier lifetimes of the samples were tested by a microwave detected photoconductivity MDPmap (Freiberg Instrument GmbH). The reflection spectra were measured by an integrating sphere (PerkinElmer Lambda750). The  $J$ – $V$  properties of the solar cells were tested by a simulated solar spectrum from a Newport 91160 solar simulator (AM 1.5G, 100 mW/cm<sup>2</sup>). The EQE data were measured by a Newport monochromator and a Keithley source meter (model 4200). A programmable electrometer (Keithley model 6514) was adopted to test the open-circuit voltage and short-circuit current of the TENG.

## ASSOCIATED CONTENT

### Supporting Information

The Supporting Information is available free of charge on the ACS Publications website at DOI: 10.1021/acsnano.8b00416.

Additional information (PDF)

## AUTHOR INFORMATION

### Corresponding Authors

\*E-mail (Z. Wen): wenzhen2011@suda.edu.cn.

\*E-mail (X. Sun): xhsun@suda.edu.cn.

\*E-mail (B. Sun): bqsun@suda.edu.cn.

### ORCID

Yuqiang Liu: 0000-0003-3494-6390

Zhen Wen: 0000-0001-9780-6876

Xuhui Sun: 0000-0003-0002-1146

Shuit-Tong Lee: 0000-0003-1238-9802

Baoquan Sun: 0000-0002-4507-4578

### Author Contributions

<sup>†</sup>Y. Liu and N. Sun contributed equally to this work.

### Notes

The authors declare no competing financial interest.

## ACKNOWLEDGMENTS

This work was supported by the National Key Research and Development Program of China (2016YFA0202402), the National Natural Science Foundation of China (91123005, 61674108, 21274087, 61504089, U1432249), the Priority Academic Program Development of Jiangsu Higher Education Institutions (PAPD), the 111 Projects, and Collaborative Innovation Center of Suzhou Nano Science and Technology. Z.W. thanks the support from China Postdoctoral Science Foundation (2017M610346) and Natural Science Foundation of Jiangsu Province of China (BK20170343). Y.L. thanks the support from Postgraduate Research & Practice Innovation Program of Jiangsu Province (KYCX17\_2043).

## REFERENCES

- (1) Polman, A.; Knight, M.; Garnett, E. C.; Ehrler, B.; Sinke, W. C. Photovoltaic Materials: Present Efficiencies and Future Challenges. *Science* **2016**, *352*, aad4424.
- (2) Wang, Z. L. On Maxwell's Displacement Current for Energy and Sensors: the Origin of Nanogenerators. *Mater. Today* **2017**, *20*, 74–82.
- (3) Wen, Z.; Yeh, M.-H.; Guo, H.; Wang, J.; Zi, Y.; Xu, W.; Deng, J.; Zhu, L.; Wang, X.; Hu, C.; Zhu, L.; Sun, X.; Wang, Z. L. Self-Powered Textile for Wearable Electronics by Hybridizing Fiber-Shaped Nanogenerators, Solar Cells, and Supercapacitors. *Sci. Adv.* **2016**, *2*, e1600097.
- (4) Chen, J.; Huang, Y.; Zhang, N.; Zou, H.; Liu, R.; Tao, C.; Fan, X.; Wang, Z. L. Micro-Cable Structured Textile for Simultaneously Harvesting Solar and Mechanical Energy. *Nat. Energy* **2016**, *1*, 16138.
- (5) Wen, Z.; Shen, Q.; Sun, X. Nanogenerators for Self-Powered Gas Sensing. *Nano-Micro Lett.* **2017**, *9*, 45.
- (6) Sun, N.; Wen, Z.; Zhao, F.; Yang, Y.; Shao, H.; Zhou, C.; Shen, Q.; Feng, K.; Peng, M.; Li, Y.; Sun, X. All Flexible Electrospun Papers Based Self-Charging Power System. *Nano Energy* **2017**, *38*, 210–217.
- (7) Wang, Z. L.; Chen, J.; Lin, L. Progress in Triboelectric Nanogenerators as a New Energy Technology and Self-Powered Sensors. *Energy Environ. Sci.* **2015**, *8*, 2250–2282.
- (8) Fan, F.-R.; Tian, Z.-Q.; Wang, Z. L. Flexible Triboelectric Generator. *Nano Energy* **2012**, *1*, 328–334.
- (9) Tang, Q.; Wang, X.; Yang, P.; He, B. A Solar Cell That Is Triggered by Sun and Rain. *Angew. Chem., Int. Ed.* **2016**, *55*, 5243–5246.

- (10) Zheng, L.; Lin, Z.-H.; Cheng, G.; Wu, W.; Wen, X.; Lee, S.; Wang, Z. L. Silicon-Based Hybrid Cell for Harvesting Solar Energy and Raindrop Electrostatic Energy. *Nano Energy* **2014**, *9*, 291–300.
- (11) Zheng, L.; Cheng, G.; Chen, J.; Lin, L.; Wang, J.; Liu, Y.; Li, H.; Wang, Z. L. A Hybridized Power Panel to Simultaneously Generate Electricity from Sunlight, Raindrops, and Wind around the Clock. *Adv. Energy Mater.* **2015**, *5*, 1501152.
- (12) Jeon, S.-B.; Kim, D.; Yoon, G.-W.; Yoon, J.-B.; Choi, Y.-K. Self-Cleaning Hybrid Energy Harvester to Generate Power from Raindrop and Sunlight. *Nano Energy* **2015**, *12*, 636–645.
- (13) Liu, Q.; Ishikawa, R.; Funada, S.; Ohki, T.; Ueno, K.; Shirai, H. Highly Efficient Solution-Processed Poly(3,4-ethylenedioxythiophene):Poly(styrenesulfonate)/Crystalline-Silicon Heterojunction Solar Cells with Improved Light-Induced Stability. *Adv. Energy Mater.* **2015**, *5*, 1500744.
- (14) Zhang, X.; Yang, D.; Yang, Z.; Guo, X.; Liu, B.; Ren, X.; Liu, S. Improved PEDOT: PSS/c-Si Hybrid Solar Cell Using Inverted Structure and Effective Passivation. *Sci. Rep.* **2016**, *6*, 35091.
- (15) Yu, P.; Tsai, C.-Y.; Chang, J.-K.; Lai, C.-C.; Chen, P.-H.; Lai, Y.-C.; Tsai, P.-T.; Li, M.-C.; Pan, H.-T.; Huang, Y.-Y.; Wu, C.-I.; Chueh, Y.-L.; Chen, S.-W.; Du, C.-H.; Horng, S.-F.; Meng, H.-F. 13% Efficiency Hybrid Organic/Silicon-Nanowire Heterojunction Solar Cell via Interface Engineering. *ACS Nano* **2013**, *7*, 10780–10787.
- (16) Liu, Y.; Zhang, Z.-G.; Xia, Z.; Zhang, J.; Liu, Y.; Liang, F.; Li, Y.; Song, T.; Yu, X.; Lee, S.-T.; Sun, B. High Performance Nanostructured Silicon-Organic Quasi *p-n* Junction Solar Cells via Low-Temperature Deposited Hole and Electron Selective Layer. *ACS Nano* **2016**, *10*, 704–712.
- (17) He, L.; Jiang, C.; Wang, H.; Lai, D. High Efficiency Planar Si/Organic Heterojunction Hybrid Solar Cells. *Appl. Phys. Lett.* **2012**, *100*, 073503.
- (18) He, J.; Gao, P.; Yang, Z.; Yu, J.; Yu, W.; Zhang, Y.; Sheng, J.; Ye, J.; Amine, J. C.; Cui, Y. Silicon/Organic Hybrid Solar Cells with 16.2% Efficiency and Improved Stability by Formation of Conformal Heterojunction Coating and Moisture-Resistant Capping Layer. *Adv. Mater.* **2017**, *29*, 1606321.
- (19) Avasthi, S.; Lee, S.; Loo, Y.-L.; Sturm, J. C. Role of Majority and Minority Carrier Barriers Silicon/Organic Hybrid Heterojunction Solar Cells. *Adv. Mater.* **2011**, *23*, 5762–5766.
- (20) Liu, Y.; Zhang, J.; Wu, H.; Cui, W.; Wang, R.; Ding, K.; Lee, S.-T.; Sun, B. Low-Temperature Synthesis TiO<sub>x</sub> Passivation Layer for Organic-Silicon Heterojunction Solar Cell with a High Open-Circuit Voltage. *Nano Energy* **2017**, *34*, 257–263.
- (21) Liu, R.; Lee, S. T.; Sun, B. 13.8% Efficiency Hybrid Si/Organic Heterojunction Solar Cells with MoO<sub>3</sub> Film as Antireflection and Inversion Induced Layer. *Adv. Mater.* **2014**, *26*, 6007–6012.
- (22) Thomas, J. P.; Leung, K. T. Defect-Minimized PEDOT: PSS/Planar-Si Solar Cell with Very High Efficiency. *Adv. Funct. Mater.* **2014**, *24*, 4978–4985.
- (23) He, J.; Yang, Z.; Liu, P.; Wu, S.; Gao, P.; Wang, M.; Zhou, S.; Li, X.; Cao, H.; Ye, J. Enhanced Electro-Optical Properties of Nanocone/Nanopillar Dual-Structured Arrays for Ultrathin Silicon/Organic Hybrid Solar Cell Applications. *Adv. Energy Mater.* **2016**, *6*, 1501793.
- (24) Yoon, S.-S.; Khang, D.-Y. High Efficiency (>17%) Si-Organic Hybrid Solar Cells by Simultaneous Structural, Electrical, and Interfacial Engineering via Low-Temperature Processes. *Adv. Energy Mater.* **2017**, 1702655.
- (25) Jeong, S.; Garnett, E. C.; Wang, S.; Yu, Z.; Fan, S.; Brongersma, M. L.; McGehee, M. D.; Cui, Y. Hybrid Silicon Nanocone-Polymer Solar Cells. *Nano Lett.* **2012**, *12*, 2971–2976.
- (26) Yu, X.; Shen, X.; Mu, X.; Zhang, J.; Sun, B.; Zeng, L.; Yang, L.; Wu, Y.; He, H.; Yang, D. High Efficiency Organic/Silicon-Nanowire Hybrid Solar Cells: Significance of Strong Inversion Layer. *Sci. Rep.* **2015**, *5*, 17371.
- (27) Pudasaini, P. R.; Ruiz-Zepeda, F.; Sharma, M.; Elam, D.; Ponce, A.; Ayon, A. A. High Efficiency Hybrid Silicon Nanopillar-Polymer Solar Cells. *ACS Appl. Mater. Interfaces* **2013**, *5*, 9620–9627.
- (28) Jeong, H.; Song, H.; Pak, Y.; Kwon, I. K.; Jo, K.; Lee, H.; Jung, G. Y. Enhanced Light Absorption of Silicon Nanotube Arrays for Organic/Inorganic Hybrid Solar Cells. *Adv. Mater.* **2014**, *26*, 3445–3450.
- (29) Lee, Y.-T.; Lin, F.-R.; Chen, C.-H.; Pei, Z. A 14.7% Organic/Silicon Nanoholes Hybrid Solar Cell via Interfacial Engineering by Solution-Processed Inorganic Conformal Layer. *ACS Appl. Mater. Interfaces* **2016**, *8*, 34537–34545.
- (30) Chen, T.-G.; Huang, B.-Y.; Chen, E.-C.; Yu, P.; Meng, H.-F. Micro-Textured Conductive Polymer/Silicon Heterojunction Photovoltaic Devices with High Efficiency. *Appl. Phys. Lett.* **2012**, *101*, 033301.
- (31) Wei, W.-R.; Tsai, M.-L.; Ho, S.-T.; Tai, S.-H.; Ho, C.-R.; Tsai, S.-H.; Liu, C.-W.; Chung, R.-J.; He, J.-H. Above-11%-Efficiency Organic-Inorganic Hybrid Solar Cells with Omnidirectional Harvesting Characteristics by Employing Hierarchical Photon-Trapping Structures. *Nano Lett.* **2013**, *13*, 3658–3663.
- (32) Oh, J.; Yuan, H.-C.; Branz, H. M. An 18.2%-Efficient Black-Silicon Solar Cell Achieved through Control of Carrier Recombination in Nanostructures. *Nat. Nanotechnol.* **2012**, *7*, 743–748.
- (33) Zhang, J.; Song, T.; Shen, X.; Yu, X.; Lee, S.-T.; Sun, B. A 12%-Efficient Upgraded Metallurgical Grade Silicon-Organic Heterojunction Solar Cell Achieved by a Self-Purifying Process. *ACS Nano* **2014**, *8*, 11369–11376.
- (34) Smith, A. J.; Wang, C.; Guo, D.; Sun, C.; Huang, J. Repurposing Blu-Ray Movie Discs as Quasi-Random Nanoimprinting Templates for Photon Management. *Nat. Commun.* **2014**, *5*, 5517.
- (35) Erickson, A. S.; Zohar, A.; Cahen, D. *n*-Si-Organic Inversion Layer Interfaces: A Low Temperature Deposition Method for Forming a *p-n* Homo Junction in *n*-Si. *Adv. Energy Mater.* **2014**, *4*, 1301724.
- (36) Sze, S. M. *Semiconductor Devices: Physics and Technology*; John Wiley & Sons, 2008.
- (37) Xue, G.; Xu, Y.; Ding, T.; Li, J.; Yin, J.; Fei, W.; Cao, Y.; Yu, J.; Yuan, L.; Gong, L. Water-Evaporation-Induced Electricity with Nanostructured Carbon Materials. *Nat. Nanotechnol.* **2017**, *12*, 317–321.
- (38) Lin, Z. H.; Cheng, G.; Lee, S.; Pradel, K. C.; Wang, Z. L. Harvesting Water Drop Energy by a Sequential Contact-Electrification and Electrostatic-Induction Process. *Adv. Mater.* **2014**, *26*, 4690–4696.
- (39) Lin, Z. H.; Cheng, G.; Lin, L.; Lee, S.; Wang, Z. L. Water-Solid Surface Contact Electrification and its Use for Harvesting Liquid-Wave Energy. *Angew. Chem., Int. Ed.* **2013**, *52*, 12545–12549.
- (40) Chun, J.; Ye, B. U.; Lee, J. W.; Choi, D.; Kang, C.-Y.; Kim, S.-W.; Wang, Z. L.; Baik, J. M. Boosted Output Performance of Triboelectric Nanogenerator via Electric Double Layer Effect. *Nat. Commun.* **2016**, *7*, 12985.